

https://dspace.org/

Experimental study on transient and steadystate impinging jet cooling condition with TiO2Water nanofluids

N Wilken; Mohsen Sharifpur; E Atofaratti; J Meyer

https://hdl.handle.net/10539/40594
WOS

Downloaded from a DSpace repository. https://dspace.org/

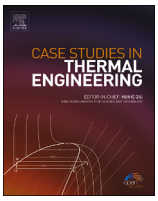
Case Studies in Thermal Engineering 57 (2024) 104301



Contents lists available at ScienceDirect

Case Studies in Thermal Engineering

journal homepage: www.elsevier.com/locate/csite



Experimental study on transient and steady-state impinging jet cooling condition with TiO_2-Water nanofluids

Nicolas Wilken [a], Mohsen Sharifpur [a, b, c, *], Emmanuel O. Atofarati [a], Josua P. Meyer [a, d]

[a] Department of Mechanical and Aeronautical Engineering, University of Pretoria, Pretoria, Private Bag X20, Hatfield, 0028, South Africa
[b] School of Mechanical, Industrial and Aeronautical Engineering, University of the Witwatersrand, Private Bag 3, Wits 2050, South Africa
[c] Department of Medical Research, China Medical University Hospital, China Medical University, Taichung, Taiwan
[d] Department of Mechanical and Mechatronic Engineering, Stellenbosch University, Stellenbosch, South Africa

ARTICLE INFO

Handling Editor: Huihe Qiu

Keywords:
Nanofluids
Jet-impingement
TiO_2
Steady-state cooling
Transient cooling
Heat transfer enhancement

ABSTRACT

Effective thermal management is crucial for optimum performance and energy conservation in energy-intensive industries and power systems. This study explores the influence of TiO_2-water nanofluids on enhancing heat transfer during impinging jet-cooling of a heated copper surface, both under transient and steady-state cooling conditions. TiO_2-water nanofluids, with volume fractions (0.025 vol% $\leq \phi \leq$ 1 vol%), were prepared, characterized, and utilized in the investigation. The experimental setup involved a dimensionless nozzle-to-target gap (H/D = 4) and Reynolds number (10000 < Re < 30000), with transient cooling behavior tracked through a dimensionless cooling curve. The TiO_2-water nanofluids demonstrated significant thermal enhancement of 14.75% and 16% at ϕ = 0.05 vol% and Re ≈ 22000, outperforming DI water in both steady-state and transient cooling conditions, respectively. The result also shows that heat transfer rates increase with higher Reynolds numbers but follow an ascent and descent pattern with increasing nanofluid volume fractions. Notably, for volume fractions exceeding ϕ = 0.1%, the nanofluid exhibited reduced heat transfer efficiency compared to DI water. The acquired data have been utilized to establish a correlation for estimating the Nusselt number as a function of Reynolds number and fluid volume fraction.

1. Introduction

In pursuit of sustainable and energy-efficient solutions, the efficient dissipation of heat stands as a paramount challenge, especially within energy-intensive industries and power systems. As the world progresses towards the ambitious Sustainable Energy Goal for 2030, the imperative for effective thermal management within these energy sectors becomes increasingly evident. This need arises in response to the rising demand for energy driven by innovative designs [1]. Impinging jets are a well-established technique with remarkable potential for achieving improved heat transfer coefficients between a coolant in motion and the cooled surface. The effectiveness of this method has been demonstrated across a spectrum of applications, including electronics cooling [2], aerospace turbine systems [3], solar thermal installations [4], heat exchangers [5], and even in the field of tribology [6].

However, the quest for better heat transfer performance has led researchers to explore innovative avenues such as improved thermophysical properties, phase change mediums, magneto-hydrodynamics, electro-hydrodynamics, surface roughness, and pulsating flow, among others. To boost the thermophysical properties of common coolants, Choi and Eastman [7] suggest the addition of nanoparticles into the coolant to form nanofluids. Nanofluids represent a groundbreaking category of fluids wherein nano-sized parti-

* Corresponding author. Department of Mechanical and Aeronautical Engineering, University of Pretoria, Pretoria, Private Bag X20, Hatfield, 0028, South Africa.
E-mail address: mohsen.sharifpur@up.ac.za (M. Sharifpur).

https://doi.org/10.1016/j.csite.2024.104301
Received 18 October 2023; Received in revised form 21 January 2024; Accepted 21 March 2024
Available online 22 March 2024
2214-157X/© 2024 The Authors. Published by Elsevier Ltd. This is an open access article under the CC BY-NC-ND license (http://creativecommons.org/licenses/by-nc-nd/4.0/).

cles are suspended within a base fluid, resulting in a homogeneous colloid with modified thermophysical properties. These specially engineered nanofluids exhibit extraordinary thermal conductivities and heat transfer capabilities, making them a focal point of research interest in the field of thermal sciences. Studies by Keblinski et al. [8] and Jang et al. [9] have summarized the exceptional mechanism of heat transfer in nanofluids and ascribed this to factors such as nanoparticles' Brownian motion, interfacial layers within the fluid, conduction within the particles themselves, and the formation of nanoparticle clusters.

The synergy between impinging jet cooling and nanofluids presents an intriguing opportunity to revolutionize heat dissipation techniques, particularly for addressing high heat density points or 'hot spots' within critical energy systems. These systems encompass a diverse range of applications, including turbine blades, solar photovoltaic installations, electronic chips, and data centers, where optimal performance hinges on effective thermal management [10,11]. One significant experimental investigation by Lv et al. [12], considered the utilization of Al2O3-water nanofluids with jet impingement on the free surface of a heated copper cylinder. The study meticulously examined a range of nanofluid volume fractions ($0.5\% \leq \phi \leq 2\%$), nozzle-to-target gap dimensions ($2 \leq H/D \leq 5$), and Reynolds numbers ($4000 < Re < 13000$). Their findings revealed a compelling relationship: heat transfer increased proportionally with particle concentration but exhibited a decrease with an increasing impingement angle. Furthermore, the study highlighted an optimal heat transfer enhancement of 61.4% under specific conditions: $\phi = 2\%$, $H/D = 4$, $Re = 12000$, and at an angle normal to the cooled surface. Supporting research by Datta et al. [13] and Atofarati et al. [14] also underscores the significance of a nozzle-to-target gap dimension of $H/D = 4$ as optimal for enhancing free surface jet impingement heat transfer using either conventional fluid or nanofluids.

Tie et al. [15] did a comprehensive work on the thermal performance of Cu-water nanofluids by impinging jet arrays on the surface of a heated copper block. Their investigation indicated that nanofluids significantly improved heat transfer in the arrayed jet impingement cooling if surfactants were not used. Their findings reported a heat transfer enhancement of 6.8%. Similarly, Zhou et al. [16] explored heat transfer from a smooth and pin-finned copper surface using Ag-water nanofluids ($0.02\% \leq \phi \leq 0.12\%$). Their results demonstrated that heat dissipation from the target surface increased with the nanofluid volume fraction, especially for surfaces with pin-fins. Notably, a substantial thermal enhancement of 6.61% was reported for the $\phi = 0.12\%$ nanofluid when compared to water. Upon a comprehensive analysis of the existing body of work on nanofluid jet-impingement cooling, it becomes evident that most studies have been performed under steady-state conditions and primarily focused on nanofluids containing aluminium particles.

Recently, Akgul et al. [17] and Ekicilier [18], investigated the influence of Alumina Oxide nanoparticle shape on the thermal and entropy performance of its nanofluid using jet impingement on a curved-convex surface. They explored the impact of nanofluid volume fraction ($1.0\% \leq \phi \leq 4.0\%$) and nanoparticle shapes (cylinders, platelets, bricks, and blades) on pressure drop and heat transfer behavior in the laminar flow regime. Their findings indicated that the platelet-shaped Alumina Oxide nanoparticle with a nanofluid volume fraction of 4.0% exhibited the most significant thermal enhancement, reaching 47.63%. In a separate study, Shi et al. [3] numerically analyzed heat transfer over a cylindrical shape using confined circumferential multiple air jets, considering Reynolds numbers ($20{,}000 \leq Re \leq 35{,}000$) and jet inclination angles ($20^\circ \leq \theta \leq 45^\circ$). They observed relatively uniform local Nusselt numbers for $\theta = 20^\circ$ and 30°, with uniformity decreasing as the inclination angle increased towards 45°. They also reported that the mean Nusselt number increased with higher Reynolds numbers. Ekiciler [19] also conducted a numerical study on the thermal performance of submerged and confined $CoFe_3O_2$/water nanofluid slot jet impingement. Their results demonstrated increased Nusselt number and Darcy friction factor with rising nanofluid concentration and flow Reynolds number. Collectively, these works validate the consistent trends that the mean Nusselt number increases with higher Reynolds numbers and nanofluid concentrations [20].

Tiara et al. [21] experimentally explored the transient cooling behavior of Cu–Al layered double hydroxide (Cu–Al-LDH) nanofluids applied to a stainless-steel plate with an original temperature of 900 °C. In their investigation, various dispersants, including SDS, CTAB, PVP, and Tween 20, among others, were individually added to Cu–Al-LDH nanofluids, and the resulting cooling performance of these mixtures was compared. The results revealed that Tween 20 mixed with Cu–Al-LDH nanofluids exhibited the most efficient cooling rate, reaching 154 °C/s during the cooling process. Other studies examining the transient behavior of nanofluid jet impingement on steel surfaces include the work of Mitra et al., where they investigated the boiling thermal performance of MWCNT-water and TiO_2-water nanofluids impinged on a hot steel surface. Additionally, studies by Modak et al. [22], Santosh et al. [23], and Sarkar et al. [24] delved into the application of TiO_2-water, Al2O3-water, CuO-water, and Cu–Al-LDH nanofluids for the heat treatment of stainless steel, respectively. After reviewing prior research on transient cooling, it becomes apparent that most of these studies focus on single-phase impingement cooling, excluding the influence of boiling phenomena. Furthermore, most of these studies have centred on steel surfaces and their metallurgical heat treatment advantages, with limited exploration of other materials in single-phase cooling processes.

Contrary to the common belief regarding nanofluid jet impingement cooling, where it is often assumed that heat transfer improves with both nanoparticle concentration in the nanofluid and Reynolds number, a critical limit exists to the nanoparticle concentration necessary for optimal heat transfer enhancement. This limitation arises due to the delicate balance between thermal conductivity and viscosity as the nanoparticle concentration in the nanofluid increases. The increase in viscosity, in turn, results in a higher pressure drop, demanding increased pumping power. Jaberi et al. [25] conducted an extensive study focusing on Al_2O_3-water nanofluids and their performance with a round jet impinging on a heated circular disk. They explored a nanoparticle concentration range of 0.0198–0.0757 wt% and Reynolds numbers ranging from 4200 to 8200. Their findings revealed that heat transfer by convection increases until a specific nanoparticle concentration threshold is attained, beyond which more increases produce diminishing returns. They observed a maximum enhanced heat transfer of approximately 50% occurring at a Reynolds number of 4200 and particle concentration of 0.0597 wt%. Similar investigations were carried out by Teamah et al. [10], who both numerically and experimentally examined Al_2O_3-water nanofluids for cooling a heated stainless-steel plate. Their findings supported the trend of the heat transfer rate increasing with higher Reynolds numbers but peaking once a critical particle concentration was reached.

In previous literature, many studies related to jet impingement have studied steady-state cooling using Al_2O_3/water nanofluid. However, to the best knowledge of this author, there are no experimental studies on transient cooling of a flat copper target using TiO_2/water. Only three transient cooling studies [26–28] have been carried out using TiO_2/water. Meanwhile, these studies focused on the cooling of high-temperature steel. This study centers on examining transient and steady-state cooling utilizing TiO_2-water nanofluids. The effect of varying nanofluid volume fraction and flow Reynolds number on heat transfer performance and cooling rates was investigated. Both transient and steady-state cooling conditions were explored in this research, employing TiO_2-water nanofluids with volume fractions (0.025 vol% $\leq \phi \leq$ 1 vol%). These nanofluids were directed onto a heated copper surface with a dimensionless nozzle-to-target gap (H/D = 4) and Reynolds numbers (10000 < Re < 30000). The thermal performance assessment was conducted through the evaluation of the Nusselt number (*Nu*) and a dimensionless transient surface temperature (θ). The findings of this study will contribute significantly to bridging the existing knowledge gap in the effective utilization of TiO_2-water nanofluids for transient and steady state jet cooling applications, particularly in areas such as electronics cooling, turbine blade cooling, and solar thermal collection systems.

2. Materials and methods

2.1. Nanofluid synthesis

Concentrated TiO_2-water nanofluid with a volume concentration of 15 wt%, prepared using the one-step technique was sourced from US-Nano, USA, and featured a specified average particle size ranging from 5 to 30 nm. For experimentation, six distinct particle volume fractions (0.025, 0.05, 0.1, 0.25, 0.5, and 1 vol%) of the nanofluid were prepared by thinning the concentrated nanofluid with a predetermined volume of de-ionized water. Sodium lauryl sulphate (SDS) sourced from Sigma-Aldrich, USA, was utilized for homogenous dispersion of the nanoparticles. The dispersant's effectiveness measurement yielded a dispersion factor of 0.8. Additionally, TEM analysis was conducted on the nanofluid to visualize the nanoparticle morphology within the dispersed fluid. The TEM analysis result shown in Fig. 1 shows the shape of the nanoparticle to be spherical. Also, it confirms the TiO_2 particle size (diameter) to be between a range of 5 nm–30 nm.

To ascertain the homogeneity and stability of the nanofluid, the mixture was first stirred for 15 min with a magnetic stirrer. Subsequently, it was ultrasonicated using a Q-700 sonicator from Qsonica, USA. The sonicator was configured with an amplitude set at 70% and operated for a 30-min duration, following a pulsating cycle of 2 s off and 5 s on. This sonication procedure was applied to individual fluid samples, each with a volume of 250 ml. To prevent potential evaporation and maintain the nanoparticles within an acceptable thermal range, the glass beaker holding the nanofluid was positioned inside a constant temperature bath, set to 15 °C. This sonication process was repeated until a total volume of 10 L of nanofluid was obtained, which was then filled into the main reservoir of the experimental setup.

2.2. Stability analysis

The stability of the nanofluid was assessed by collecting two 50 ml samples, which were then subjected to desk-visualization and viscosity measurements over time. As illustrated in Fig. 2, no visible particle sedimentation occurred during the 4-h period following preparation, confirming the visual stability of the fluid. Viscosity measurements were conducted with SV-10 vibro-viscometer. The results, presented in Fig. 3, indicate that the nanofluid's viscosity remained consistently stable throughout the observed period. Based on the findings from both nanofluid samples, they were deemed to be suitably stable.

2.3. Thermophysical properties

SV-10 vibro-viscometer was also employed to measure the viscosity of different nanoparticle concentrations of prepared nanofluids at different temperatures. Prior to conducting nanofluid measurements, the viscometer underwent calibration using DI-water. Subsequently, the viscosity of both the nanofluid and DI-water was measured over a temperature spanning from 15 °C to 45 °C. The analysis results, depicted in Fig. 4, reveal that viscosity decreases as temperature rises. Moreover, the influence of nanoparticle concentration on fluid viscosity was found to be nearly negligible within the range of nanoparticle concentrations from 0 vol% to 0.25 vol%. However, for higher nanofluid volume fractions, viscosity exhibited a spontaneous increase. Notably, highly viscous fluids may result in elevated friction factors and increased pumping power requirements.

The thermal conductivity of the TiO_2-water nanofluid samples was predicted using the experimental model established by He et al. [29], as presented in equation (1). The results presented in Fig. 5 show that temperature is directly proportional to the fluid's ther-

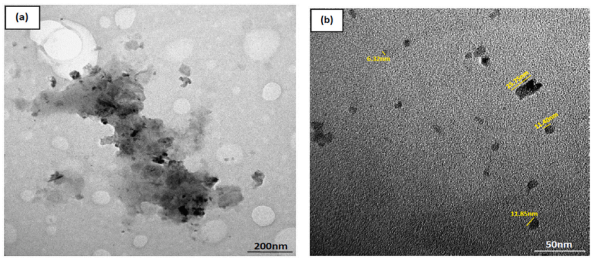
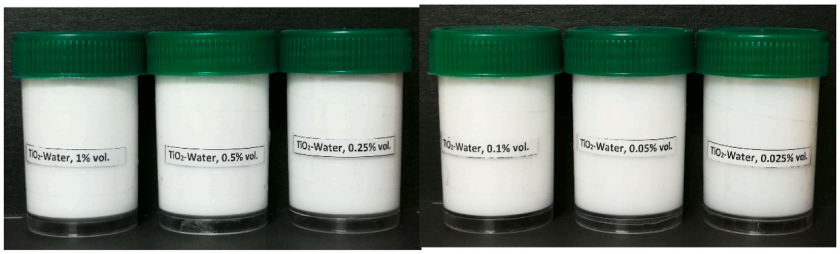
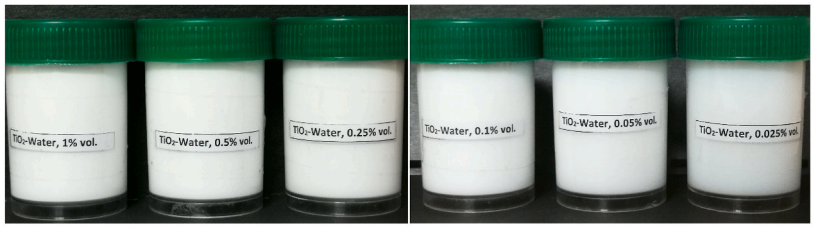


Fig. 1. TEM analysis of TiO_2 -DI water Nanofluid.



(a)



(b)

Fig. 2. Visual stability of nanofluid (a) after preparation (b) after 4 h.

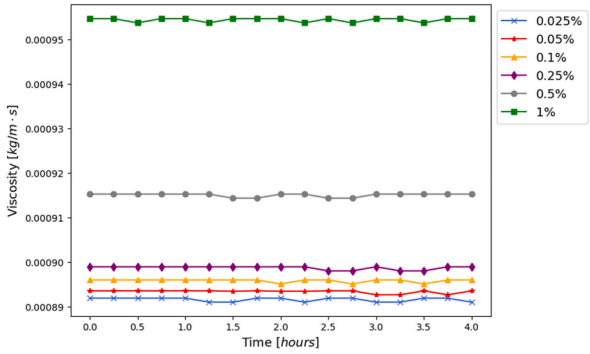


Fig. 3. Viscosity (Stability) of TiO_2-water measured with time.

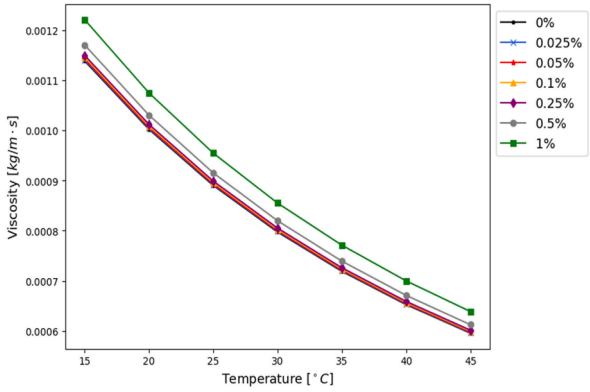


Fig. 4. Impact of Temperature change on the Viscosity of TiO_2-water.

mal conductivity. Furthermore, it revealed that thermal conductivity improves with the nanofluids volume fraction. Additionally, the density and specific heat capacity were determined using the mixing theories proposed by Cheremisinoff [30]and Pak and Cho [31], as presented in equations (2) and (3), respectively. Table 1 summarize the properties of the nanofluids and DI water obtained at the mean room temperature.

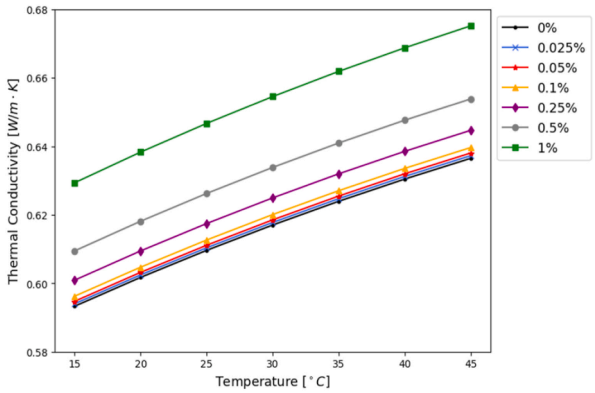


Fig. 5. Impact of Temperature change on the Thermal Conductivity of TiO_2-water.

Table 1
Summary of fluid thermophysical properties.

Fluid Property	DI water	TiO_2 Nanoparticles
Density	997.1 (kg/m^3)	4250
Specific heat	4180 (J/kg.K)	686
Viscosity	8.91 × 10^{-4} (kg/m.s)	As in Fig. 3
Thermal Conductivity	0.607 (W/m.K)	As in Fig. 4

$$k_{nf} = k_{bf} \bullet \left(125.62\varphi^2 + 4.82\varphi + 1\right) \tag{1}$$

$$\rho_{nf} = (1-\varphi)\,\rho_{bf} + \varphi\rho_{np} \tag{2}$$

$$c_{pnf} = \frac{\varphi c_{pnp}\rho_{np} + (1-\varphi)\,c_{pbf}\rho_{bf}}{\rho_{nf}} \tag{3}$$

2.4. Experimental set-up

The experimental test rig, as depicted in Fig. 6 (a), consists of four distinct subsystems: the fluid delivery system, the test section, the data acquisition system, and the safety system. The fluid delivery system comprises an array of components, including a 10-L fluid

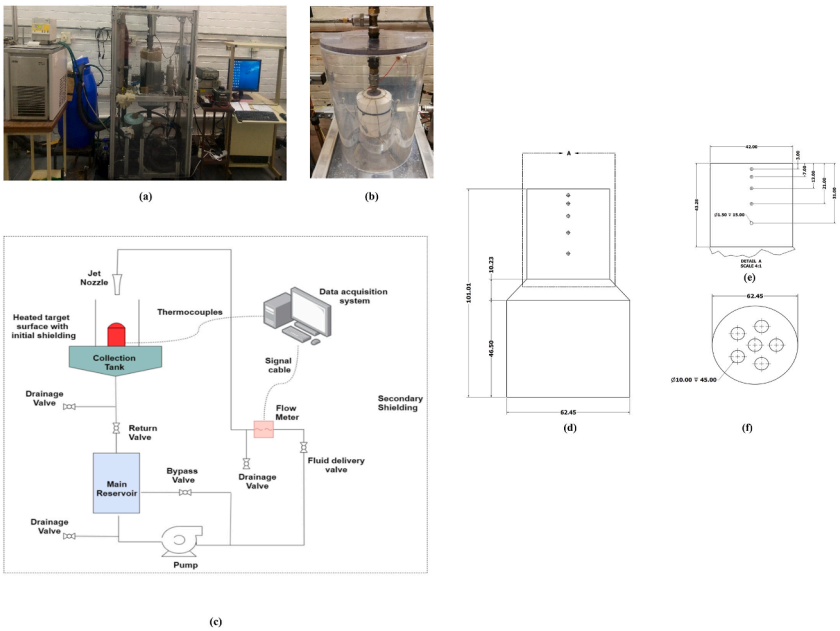


Fig. 6. Experimental test rig's (a) pictural view (b&d) copper test section, (c) schematics diagram (e) the axial thermocouple's locations, (f) position of cartridge heaters.

reservoir, a Speck centrifugal pump, an Burkert (8081) ultrasonic flow meter, a Lechler circular jet nozzle (D_{jet} = 1.65 mm), and a bespoke drainage tank. To regulate the pump's flow rate, a solid-state relay circuit was implemented to regulate the flow rate.

The test section, shown in Fig. 6 (b), (c), and **(d)**, consists of a copper block with original dimensions of 62.45 mm in diameter and 100.01 mm in length. To minimize thermal losses to the ambient surroundings, the copper bar is enclosed within a Polytetrafluoroethylene (PTFE) casing. Additionally, six cartridge heaters (Marathon Heaters INC, USA), each with a power capacity of 220 V and 100 W, are strategically placed in designated holes, as indicated in Fig. 6 (d). The heater power supply is turned on to this setting for 5 min until the surface temperature reaches 50 °C, then it is being cool with the fluid at a temperature of about 21–23 °C. The data acquisition system involves using thermocouples (Type K and T), a Data logger, and a computer system. Five shielded K-type thermocouples are positioned at several axial levels along the copper bar to capture essential thermal data required to derive the total surface heat flux and estimate the target surface's temperature during the cooling experiments. The shielded K-type thermocouples were used to ensure the thermocouple junction was not damaged during insertion into the copper bar. Also, five T-type thermocouple was placed around the target surface's perimeter to measure the exiting coolant's mean temperature. Following each experimental run, data files obtained through LabVIEW are saved and analyzed using Microsoft Excel and Python scripts.

Finally, the safety system consists of both primary and secondary shields designed to prevent unintended exposure of nanofluid and nanoparticles to the environment. The primary shield is a Perspex cylinder and lid that surrounds the nozzle and the test section. The secondary shielding, as depicted in Fig. 6 (a), consists of an outward polycarbonate cover that envelops the whole test rig, including the drain tray where the setup is positioned.

2.5. Data reduction

Throughout this study, fluid thermophysical properties were obtained using a similar set of equations used in the work of Atofarati et al. [14], among others. The bulk temperature was obtained as shown in Equation (4). In this equation, T_{jet} represents the jet exit temperature, anrepresents $\overline{T}_e$ represents the mean exit fluid temperature. Fourier's law was applied to estimate heat flux across the copper cylinder. In this calculation, k_c was considered as the cooled material's thermal conductivity (Copper), while Δx and ΔT represented the spacing and temperature differences between the corresponding thermocouple locations. Since multiple thermocouples were positioned at various locations within the specimen, a biased heat flux was calculated using Equations (5) and (6).

Subsequently, the external temperature of the target surface was estimated based on the average of the five temperature values ($T_{s,i}$) obtained using the approximation method and any of its five internal thermocouples, along with the heat flux, as shown in Equations (7) and (8), where $T_{Th,i}$ represents the temperature of each thermocouple, and $\Delta x_{s,i}$ is the gap between the surface and the location of the corresponding thermocouple. MTheaverage surface and average Nusselt number heat transfer coefficients were determined using Equations (9) and (10), respectively. Here, D_{jet} represents the nozzle diameter, while k implies the thermal conductivity of the coolant at the bulk temperature. The Reynolds number was calculated employing Equation (11). To remove the impact of the temperature of inlet fluid on the transient cooling analysis, a dimensionless transient surface temperature (θ) was introduced, as indicated in Equation (12).

$$T_b = \frac{T_{jet} + \overline{T}_e}{2} \tag{4}$$

$$\dot{q} = -k_c \bullet \frac{\Delta T}{\Delta x} \tag{5}$$

$$\dot{q}_{weight} = \frac{\sum_{i=1}^{4} (\Delta x \bullet \dot{q})_{i,i+1}}{\sum_{i=1}^{4} \Delta x_{i,i+1}} \tag{6}$$

$$T_{s,i} = T_{Th,i} - \frac{\dot{q}_{weight} \Delta x_{s,i}}{k_c} \tag{7}$$

$$\overline{T}_s = \frac{T_{s,1} + T_{s,2} + T_{s,3} + T_{s,4} + T_{s,5}}{5} \tag{8}$$

$$h = \frac{\dot{q}_{weight}}{T_s - T_{jet}} \tag{9}$$

$$Nu = h \bullet \frac{D_{jet}}{k} \tag{10}$$

$$Re = \frac{\rho \bullet U \bullet D_{jet}}{\mu} \tag{11}$$

$$\theta = \frac{T_s - T_{jet}}{T_{jet}} \tag{12}$$

2.6. Uncertainty analysis

Uncertainty analysis of the experimentally measured data was carried out using the methods presented by Moffat [32] and Dunn & Davis [33]. The uncertainty associated with fundamental parameters, including diameters, flowrate, temperature, viscosity, etc., was initially assessed in terms of bias (b_i) and precision error (p_i) using equation (14). Afterwards, other derived parameters (N), such as the Reynolds number, Nusselt number, and heat transfer coefficient, were estimated using equations (15) and (16) with a 95% confidence interval. While equations (17) and (18) shows a sample calculation formular for uncertainty in Reynold number and Nusselt number respectively. The results of the uncertainty analysis are briefly presented in Table 2.

$$\delta x_i = \left[(b_i)^2 + (p_i)^2 \right]^{\frac{1}{2}} \tag{14}$$

$$N = N\left(x_1, x_2, x_3, \ldots\ x_n\right) \tag{15}$$

$$\delta N = \left[\left(\frac{\partial N}{\partial x_1} \bullet \delta x_1 \right)^2 + \left(\frac{\partial N}{\partial x_2} \bullet \delta x_2 \right)^2 + \left(\frac{\partial N}{\partial x_3} \bullet \delta x_3 \right)^2 + \ldots + \left(\frac{\partial N}{\partial x_n} \bullet \delta x_n \right)^2 \right]^{\frac{1}{2}} \tag{16}$$

$$\delta Re = \left[\left(\frac{\partial Re}{\partial \rho} \bullet \delta \rho \right)^2 + \left(\frac{\partial Re}{\partial U} \bullet \delta U \right)^2 + \left(\frac{\partial Re}{\partial D_{jet}} \bullet \delta D_{jet} \right)^2 + \left(\frac{\partial Re}{\partial \mu} \bullet \delta \mu \right)^2 \right]^{\frac{1}{2}} \tag{17}$$

$$\delta Nu = \left[\left(\frac{\partial Nu}{\partial h} \bullet \delta h \right)^2 + \left(\frac{\partial Nu}{\partial D_{jet}} \bullet \delta D_{jet} \right)^2 + \left(\frac{\partial Nu}{\partial k} \bullet \delta k \right)^2 \right]^{\frac{1}{2}} \tag{18}$$

3. Experimental procedure

The experimental investigation focused on analysing steady-state and transient cooling of a heated copper cylinder using DI-water and various volume fractions of TiO2-water nanofluids (0.025%, 0.05%, 0.1%, 0.25%, 0.5%, and 1%). For steady-state jet impingement tests, the heating process involved introducing the heat transfer fluid (HTF) into the main reservoir, adjusting the power dial for six cartridge heaters (approximately 145 W), and monitoring the temperature using LabView-connected thermocouples. The copper specimen was then elevated to 50 °C over 5 min. The power dial controlling the centrifugal pump was adjusted for the desired volume flow rate, and impingement cooling was initiated at a constant surface heat flux. Steady-state conditions were typically achieved within the first minute, and cooling data was recorded for 3 min. Post-run procedures included opening the return valve for HTF return, cooling the fluid to 21–23 °C, and repeating each test at least three times for reliability.

For transient state jet impingement tests, the copper specimen was heated to 105 °C, heaters were turned off, and impingement cooling was initiated. Thermal data was recorded until the surface temperature dropped below 40 °C, with a maximum pump power setting of 100% due to time sensitivity. The temperature data were non-dimensionalized for analysis and plot.

In post-testing procedures, fluid handling involved pumping fluid to the drainage tank, draining, and using additional drainage valves for optimal fluid collection. A cleaning process included pumping distilled water through the system, repeated for preventing particle deposition. The copper target surface was also cleaned of residual nanoparticles and impurities. This comprehensive procedure ensured reliable and repeatable experimental data for each HTF.

4. Results and discussion

4.1. Verification of the experimental model

Before conducting experiments with the TiO_2-water nanofluid, validation of the experimental test rig was initially done using previous experimental data involving jet impingement cooling with DI water. To accomplish this, the Nusselt number (*Nu*) correlations

Table 2
Uncertainty in Measured and calculated Parameters.

Thermo-fluid Parameter	Symbol (unit)	Max. Uncertainty
Flow rate	$\dot{Q}$ (kg/s)	2.0%
Temperature	T (kg/m^3)	0.047%
Ammeter	I (A)	2.0%
Diameter	D (m)	2.0%
Voltmeter	V (volt)	1.7%
Thermal conductivity	k (W/m.K)	2.03%
Viscosity	μ (kg/m.s)	1%
Reynolds number	–	2.24%
Heat transfer coefficient	h (W/m^2.K)	3.33%
Heat flux	q (W/m^2)	0.16%
Nusselt number	–	4.08%

(Equation (16) and (17)) from the experimental and analytical studies on free surface circular normal jet impingement heat transfer on flat surfaces conducted by Zhao et al. [34] was compared with the experimental Nusselt number values obtained in this test rig.

The plot illustrating the experimental Nusselt number against the Reynolds number, as presented in Fig. 7, reveals that equation (16) closely approximated the experimental results obtained from this test rig, especially as the Reynolds number increased. An absolute error of 0.5 and 25%, was observed which may be attributed to the model's failure, because of certain parameters, such as the nozzle-to-target gap, which can impact jet impingement heat transfer, but were not accounted for in the correlations. Conversely, Equation (17) consistently overpredicted the Nusselt number as the Reynolds number increased. Based on the close agreement with equation (16), the experimental test rig's performance is valid. The verification corresponds with the results of Zhao et al. as the correlation slightly overpredicts the experimental data in their study. However, Equation (16) over predicted in this case, while Equation (17) slightly fits.

$$Nu = 0.7212\left(\frac{2d}{D}\right)^{2} Pr^{0.4}\, Re^{0.5} + 0.89\left(\frac{2d}{D}\right)^{2}\left[\left(\frac{D}{2d}\right)^{3/2} - 1\right] Pr^{1/3}\, Re^{0.5} \tag{19}$$

$$Nu = 0.9454 Pr^{1/3}\, Re^{0.43} \tag{20}$$

4.2. Steady-state cooling with TiO_2-water nanofluids jet

As depicted in Fig. 8, the results clearly demonstrate a direct proportionality between the average Nusselt numbers and the flow Reynolds numbers for all the TiO_2 nanoparticle concentrations considered under steady-state conditions. This behaviour aligns with typical observations by previous researchers on impinging jet cooling studies. It is often attributed to an improvement in the heat transfer coefficient due to a higher fluid flow rate [14].

While assessing the effect of particle concentration on thermal augmentation in jet impingement tests, it became evident that nanofluids led to enhanced heat transfer for specific nanoparticle concentrations (ϕ = 0.05% and 0.1%) when compared to DI water. Interestingly, the nanofluid with a volume fraction of ϕ = 0.025% exhibited performance nearly equivalent to that of DI water. However, the heat transfer performance for nanofluids with volume fractions ranging from 0.25 to 1% was unfavourable. This decline in heat transfer performance can be attributed to the previously mentioned compromise between nanofluid's viscosity and thermal con-

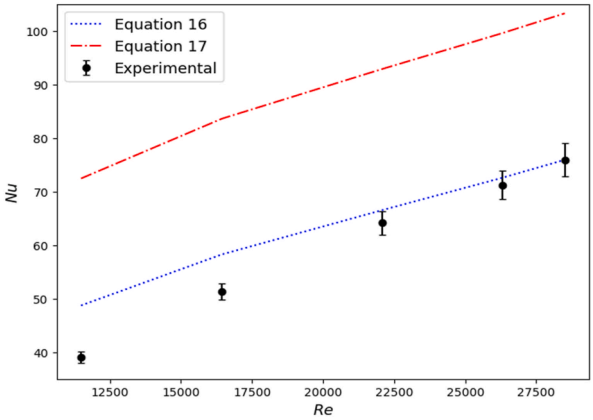


Fig. 7. Verification of Test rig considering steady-state cooling with DI water.

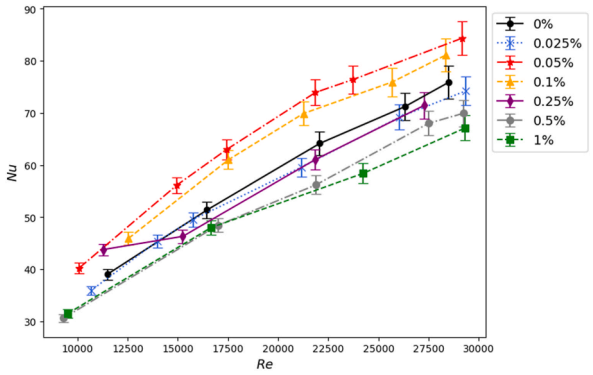


Fig. 8. Mean Nusselt numbers against Reynolds number for the varying volume fraction of TiO_2 (ϕ = 0 to ϕ = 1%) in the steady-state condition.

ductivity as nanoparticle concentration increases. At these higher nanofluid volume fractions, the viscosity effect outweighs the thermal conductivity effect, leading to reduced Reynolds numbers and, consequently, decreased heat transfer rates.

To provide further insight into the adverse effects observed in jet-impingement cooling with high nanoparticle concentration nanofluids, the findings by Tie et al. [15] and Jaberi et al. [25] support this outcome. This study indicates that a rise in nanoparticle volume fraction results in higher fluid viscosity and, subsequently, an increased boundary layer thickness. The experimental data in Fig. 8 also reveals that a peak average Nusselt number enhancements was 14.75%, for the 0.05% volume fraction, while a reduction of 13.05% was observed for the 1% volume fraction of the nanofluid at Re ≈ 22,000.

4.3. Correlation development for steady state cooling

Utilizing the experimental data presented graphically in Fig. 8, a mathematical correlation was developed, as shown in Equation (18), to describe the connection between the Nusselt number (*Nu*), Reynolds number (Re), and the nanofluid volume fraction (ϕ) through regression analysis. The coefficient of determination (R^2) for this correlation was determined to be 98%.

Fig. 9 offers a visual contrast between the measured and determined (empirical) Nusselt numbers for the impingement heat transfer tests. The proposed empirical Nusselt number, derived from

$$Nu = \begin{cases} 0.1263 \bullet Re^{0.705}\phi^{0.235}, \phi < 0.1\% \\ 0.0669 \bullet Re^{0.67}\phi^{-0.1}, \phi \geq 0.1\% \end{cases} \quad (21)$$

Equation (18) demonstrated the ability to forecast the experimental Nusselt number within a narrow error range of ±10%. Consequently, equation (18) proved to be a highly accurate tool for predicting the Nusselt number of TiO_2-water nanofluid in the context of a single circular nozzle-impinging jet.

4.4. Transient TiO_2-water nanofluids impingement cooling

The transient jet cooling investigated in this study simulates emergency cooling after quenching the heat source. Initially, the test section was heated to a predetermined mean surface temperature of 105 °C, after which the power supply was turned off, and the cooling process was initiated until a temperature below 40 °C was attained, neglecting the boiling effect. The dimensionless target-surface temperature results were plotted against cooling time, as illustrated in Fig. 10. These plots depict the transient cooling curves for various TiO_2-water nanofluids volume fractions. To ensure consistency, the transient cooling data were dimensionless, eliminating the impact of the inlet jet temperature on the overall cooling behaviour.

Upon analysing the figure, it becomes evident that the transient cooling performance of TiO_2-water nanofluids is a similar pattern to the steady-state cooling performance. Similarly, for high nanofluid volume fraction ($0.25 \leq \phi \leq 1\%$), cooling efficiency declined compared to DI-water at the same flow condition. Conversely, for particle fractions ($\phi \leq 0.1\%$), the opposite effect was noticed, with improved cooling efficiency. Specifically, during transient jet cooling with TiO_2-water nanofluid volume fractions of 0.025, 0.05, and 0.1%, dimensionless cooling effectiveness was enhanced by about 6%, 16%, and 8%, respectively. Consequently, the study resolved that the peak enhancement occurred while utilizing TiO_2-water nanofluid with a volume fraction of 0.05%.

While most literature suggests that enhanced heat transfer is primarily due to increased nanoparticle concentration leading to improved heat transfer rates, Fig. 10 signifies that the transient cooling performance in this study did not exhibit this such trend. A reasonable justification could be linked to the previously mentioned trade-off between viscosity and thermal conductivity observed in the steady-state cooling cases. Furthermore, an overly high nanofluid volume fraction may lead to significant buildup of particles on the target surface, which may potentially obstruct the heat transfer between the heat transfer fluid and the cooled specimen under examination. This occurrence can be ascribed to the notable contrast in thermal conductivity between TiO_2 and the copper target surface, offering a plausible rationale for the observed trends when volume fractions surpass 0.1%.

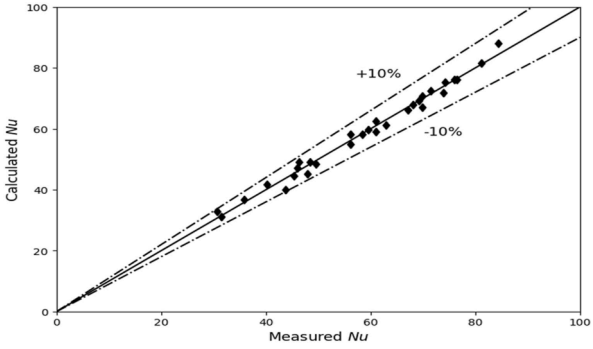


Fig. 9. Relationship between the Empirical and experimental Nusselt number.

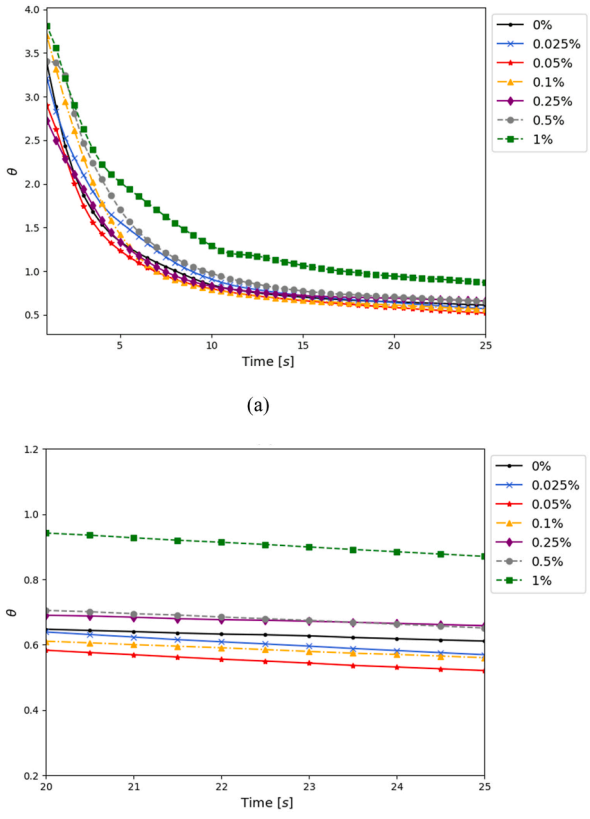


Fig. 10. Dimensionless cooling temperature against time: (a) complete cooling curve, (b) expanded cooling curve for $20 \leq t \leq 25$ s.

5. Conclusions

In this experimental investigation, the thermal performance of TiO_2-water nanofluids in both transient and steady-state jet cooling conditions was examined with nanofluid volume fractions (0.025 vol% $\leq \phi \leq$ 1 vol%), dimensionless nozzle-to-target gap (H/D = 4) and flow Reynolds numbers (10000 < Re < 30000). The key conclusions for the above-mentioned range are as follows:

i. Reynolds Number Impact:

a. Heat transfer in nanofluid jet impingement was directly proportional to the Reynolds number, primarily due to enhanced convection resulting from higher fluid flow rates.

ii. Nanofluid Enhancement:

a. The use of TiO_2-water nanofluids demonstrated a clear advantage in improving overall heat transfer during free-surface jet impingement cooling.
b. The highest average Nusselt number enhancement observed was approximately 14.75%, achieved with a particle concentration of 0.05%.
c. High volume fraction of the nanofluid had an adverse effect on heat transfer.

iii. Correlation Development:

a. A predictive correlation for average Nusselt numbers of TiO_2-water nanofluids jet impingement cooling was proposed.
b. This correlation demonstrated excellent accuracy, with predictions matching experimental data within a margin of less than 10%.

iv. Transient Cooling Efficiency:

a. In transient cooling scenarios, nanofluid concentrations below 0.1% showed improved cooling efficiency for copper specimens, while higher concentrations had adverse effects.
b. The optimal particle volume fraction was determined to be 0.05%, resulting in a remarkable 16% enhancement in cooling efficiency.

These findings highlight the potential of TiO_2-water nanofluids to improve heat transfer in impinging jet cooling, with implications for various engineering applications, such as advanced cooling systems for electronic devices, high-performance thermal management in aerospace technologies, and improved efficiency in solar thermal systems.

CRediT authorship contribution statement

Nicolas Wilken: Data curation, Formal analysis, Investigation, Writing – original draft. **Mohsen Sharifpur:** Conceptualization, Funding acquisition, Methodology, Project administration, Resources, Supervision, Writing – review & editing. **Emmanuel O. Atofarati:** Formal analysis, Investigation, Writing – original draft. **Josua P. Meyer:** Funding acquisition, Resources, Supervision, Writing – review & editing.

Declaration of competing interest

The authors declare that they have no known competing financial interests or personal relationships that could have appeared to influence the work reported in this paper.

Data availability

Data will be made available on request.

Acknowledgements

This research is a part of a project which was funded by the Technology Innovation Agency (TIA), an implementing entity of the RSA Department of Science and Technology which is duly acknowledged and appreciated. The authors would like to appreciate all the kind assistance from the Department of Research & Innovation Support of the University of Pretoria.

Nomenclature

Symbols

T	Temperature °C or K
D or d	Diameter mm
h	Heat transfer coefficient $W/m^2 \bullet K$
c_p	Specific heat $J/kg \bullet K$
$\dot{q}$	Heat flux W/m^2
k	Thermal conductivity $W/m \bullet K$
U	Velocity m/s

Dimensionless Parameters

Re	Reynolds number
Pr	Prandtl number
Nu	Nusselt number
H/D	Nozzle-to target gap/nozzle diameter
θ	dimensionless transient surface temperature

Greek Letters

μ	Dynamic viscosity $kg/m \bullet s$
ρ	Density kg/m^3
ϕ	Volume fraction %

Subscripts

b	Bulk fluid
bf	Base fluid
nf	Nanofluid
c	Copper
e	Exit
i	index
np	Nanoparticle
Th	Thermocouple
weight	Weighted

Abbreviations

DI	De-ionized
HTC	Heat transfer coefficient
HTF	Heat transfer fluid

References

[1] S. D. United nations, “Goal 7 | Department of Economic and Social Affairs.” https://sdgs.un.org/goals/goal7 (accessed October. 3, 2023).
[2] A. Siricharoenpanich, S. Wiriyasart, P. Naphon, Study on the thermal dissipation performance of GPU cooling system with nanofluid as coolant, Case Stud. Therm. Eng. 25 (Jun. 2021) 100904, https://doi.org/10.1016/J.CSITE.2021.100904.
[3] L. Shi, X. Zhu, Z. Du, Study on convective heat transfer characteristics of inclined jet impinging cylindrical target surface in the confined space, Appl. Therm. Eng. 218 (Jan. 2023) 119316, https://doi.org/10.1016/J.APPLTHERMALENG.2022.119316.
[4] S. Maatoug, et al., Pulsating multiple nano-jet impingement cooling system design by using different nanofluids for photovoltaic (PV) thermal management, Case Stud. Therm. Eng. 41 (Jan) (2023), https://doi.org/10.1016/J.CSITE.2022.102650.
[5] Z. Tang, C. Yin, R. Sun, J. Cheng, Study on the flow and heat transfer of a nanofluid hybrid jet impinging on a corrugated microchannel heat sink, Int. J. Therm. Sci. 194 (Dec. 2023) 108590, https://doi.org/10.1016/J.IJTHERMALSCI.2023.108590.
[6] J.D. Benther, S. Gunasekera, P. Lappas, G. Rosengarten, Surface durability during high-speed spray impingement onto heat-exchanger materials and modified surfaces, Tribol. Int. 181 (Mar. 2023) 108297, https://doi.org/10.1016/J.TRIBOINT.2023.108297.
[7] S.U.S. Choi, S. Li, J.A. Eastman, Measuring thermal conductivity of fluids containing Oxide nanoparticles, J. Heat Tran. 121 (2) (May 1999) 280–289, https://doi.org/10.1115/1.2825978.
[8] P. Keblinski, S.R. Phillpot, S.U.S. Choi, J.A. Eastman, Mechanisms of heat flow in suspensions of nano-sized particles (nanofluids), Int. J. Heat Mass Tran. 45 (4) (Feb. 2002) 855–863, https://doi.org/10.1016/S0017-9310(01)00175-2.
[9] S.P. Jang, S.U.S. Choi, Effects of various parameters on nanofluid thermal conductivity, J. Heat Tran. 129 (5) (May 2007) 617–623, https://doi.org/10.1115/1.2712475.
[10] M.A. Teamah, M.M. Khairat Dawood, A. Shehata, Numerical and experimental investigation of flow structure and behavior of nanofluids flow impingement on horizontal flat plate, Exp. Therm. Fluid Sci. 74 (Jun. 2016) 235–246, https://doi.org/10.1016/J.EXPTHERMFLUSCI.2015.12.012.
[11] E.O. Atofarati, M. Sharifpur, J.P. Meyer, Pulsating nanofluid-jet impingement cooling and its hydrodynamic effects on heat transfer, Int. J. Therm. Sci. 198 (1) (January 2024) 108874, https://doi.org/10.1016/j.ijthermalsci.2023.108874.
[12] J. Lv, S. Chang, C. Hu, M. Bai, P. Wang, K. Zeng, Experimental investigation of free single jet impingement using Al2O3-water nanofluid, Int. Commun. Heat Mass Tran. 88 (Nov. 2017) 126–135, https://doi.org/10.1016/J.ICHEATMASSTRANSFER.2017.08.017.
[13] A. Datta, S. Kumar, P. Halder, Heat transfer and thermal characteristics effects on moving plate impinging from Cu-water nanofluid jet, J. Therm. Sci. 29 (1) (Apr. 2019) 182–193 https://doi.org/10.1007/S11630-019-1107-7, 2019 291.
[14] E.O. Atofarati, M. Sharifpur, J. Meyer, Hydrodynamic effects of hybrid nanofluid jet on the heat transfer augmentation, Case Stud. Therm. Eng. 51 (July) (2023) 103536, https://doi.org/10.1016/j.csite.2023.103536.
[15] P. Tie, Q. Li, Y. Xuan, Heat transfer performance of Cu–water nanofluids in the jet arrays impingement cooling system, Int. J. Therm. Sci. 77 (Mar. 2014) 199–205, https://doi.org/10.1016/J.IJTHERMALSCI.2013.11.007.
[16] M. Zhou, G. Xia, L. Chai, Heat transfer performance of submerged impinging jet using silver nanofluids, Heat Mass Transf. und Stoffuebertragung 51 (2) (Feb. 2015) 221–229, https://doi.org/10.1007/S00231-014-1387-0/FIGURES/12.
[17] V. Akgül, H. Kaya, EFFECT OF PARTICLE SHAPE ON HEAT TRANSFER AND ENTROPY GENERATION PERFORMANCE OF Al2O3/WATER NANOFLUID JET FLOW IMPINGING ON A CONVEX SURFACE, Heat Tran. Res. 54 (2) (Jan. 2023) 39–56, https://doi.org/10.1615/HEATTRANSRES.2022043452.
[18] R. Ekiciler, M.S.A. Çetinkaya, K. Arslan, Effect of shape of nanoparticle on heat transfer and entropy generation of nanofluid-jet impingement cooling, Int. J. Green Energy, Taylor Fr. Online 17 (10) (Aug. 2020) 555–567, https://doi.org/10.1080/15435075.2020.1739692.
[19] R. Ekiciler, Heat transfer enhancement of a slot-confined and submerged impinging jet utilizing lamina-shaped CoFe3O2/water nanofluid, Int. J. Energy Stud. 8 (2) (Jun. 2023) 167–187, https://doi.org/10.58559/IJES.1263940.
[20] R. Kumar, et al., Convective heat transfer enhancement using impingement jets in channels and tubes: a comprehensive review, Alex. Eng. J. 70 (2023) 349–376, https://doi.org/10.1016/j.aej.2023.02.013.
[21] A.M. Tiara, S. Chakraborty, I. Sarkar, S.K. Pal, S. Chakraborty, Heat transfer in jet impingement on a hot steel surface using surfactant based Cu–Al layered double hydroxide nanofluid, Int. J. Heat Mass Tran. 101 (Oct. 2016) 825–833, https://doi.org/10.1016/J.IJHEATMASSTRANSFER.2016.05.094.
[22] M. Modak, S.S. Chougule, S.K. Sahu, An experimental investigation on heat transfer characteristics of hot surface by using CuO-water nanofluids in circular jet impingement cooling, J. Heat Tran. 140 (1) (Jan. 2018), https://doi.org/10.1115/1.4037396/375610.
[23] K. Santosh, P. Nayak, M. Chandra, S.K.S. Parashar, S. Kumar Nayak, C. Mishra, Enhancement of Heat Transfer by Water–Al2O3 and Water–TiO2 Nanofluids Jet Impingement in Cooling Hot Steel Surface, vol. 11, Nov. 2016, pp. 1253–1273 https://doi.org/10.1080/17458080.2016.1209789, 10.1080/17458080.2016.1209789.
[24] I. Sarkar, S. Chakraborty, J.M. Jha, S.K. Pal, S. Chakraborty, Ultrafast cooling of a hot steel plate using Cu-Al layered double hydroxide nanofluid jet, Int. J. Therm. Sci. 116 (Jun. 2017) 52–62, https://doi.org/10.1016/J.IJTHERMALSCI.2017.02.009.
[25] B. Jaberi, T. Yousefi, B. Farahbakhsh, M.Z. Saghir, Experimental investigation on heat transfer enhancement due to Al2O3–water nanofluid using impingement of round jet on circular disk, Int. J. Therm. Sci. 74 (C) (Dec. 2013) 199–207, https://doi.org/10.1016/J.IJTHERMALSCI.2013.06.013.
[26] S. Mitra, S.K. Saha, S. Chakraborty, S. Das, Study on boiling heat transfer of water–TiO2 and water–MWCNT nanofluids based laminar jet impingement on heated steel surface, Appl. Therm. Eng. 37 (May 2012) 353–359, https://doi.org/10.1016/J.APPLTHERMALENG.2011.11.048.
[27] K. Santosh, P. Nayak, M. Chandra, S.K.S. Parashar, S. Kumar Nayak, C. Mishra, Enhancement of heat transfer by water–Al2O3 and water–TiO2 nanofluids jet impingement in cooling hot steel surface, J. Exp. Nanosci. 11 (16) (Nov. 2016) 1253–1273, https://doi.org/10.1080/17458080.2016.1209789.
[28] M.K. Singh, D. Yadav, S. Arpit, S. Mitra, S.K. Saha, Effect of nanofluid concentration and composition on laminar jet impinged cooling of heated steel plate, Appl. Therm. Eng. 100 (May 2016) 237–246, https://doi.org/10.1016/J.APPLTHERMALENG.2016.01.032.
[29] Y. He, Y. Men, Y. Zhao, H. Lu, Y. Ding, Numerical investigation into the convective heat transfer of TiO2 nanofluids flowing through a straight tube under the laminar flow conditions, Appl. Therm. Eng. 29 (10) (Jul. 2009) 1965–1972, https://doi.org/10.1016/J.APPLTHERMALENG.2008.09.020.
[30] N.P. Cheremisinoff, Encyclopedia of Fluid Mechanics. Vol. 3: Gas-liquid Flows, vol. 3, Gulf Pub. Co., Houston, TX, 1986.
[31] B.C. Pak, Y.I. Cho, Hydrodynamic and heat transfer study of dispersed fluids with submicron metallic oxide particles, Exp. HEAT Transf. An Int. J. 11 (2) (1998) 151–170, https://doi.org/10.1080/08916159808946559.
[32] R.J. Moffat, Describing the uncertainties in experimental results, Exp. Therm. Fluid Sci. 1 (1) (Jan. 1988) 3–17, https://doi.org/10.1016/0894-1777(88)90043-X.
[33] P.F. Dunn, M.P. Davis, Measurement and data analysis for engineering and science, in: Meas. Data Anal. Eng. Sci, fourth ed., Jan. 2017, pp. 1–574 https://doi.org/10.1201/b22182, fourth edition.
[34] Y. Zhao, T. Masuoka, T. Tsuruta, C.F. Ma, Conjugated heat transfer on a horizontal surface impinged by circular free-surface liquid jet, JSME Int. J. Ser. B Fluids Therm. Eng. 45 (2) (May 2002) 307–314, https://doi.org/10.1299/JSMEB.45.307.